Mathematical Modeling-Guided Evaluation of Biochemical, Developmental, Environmental, and Genotypic Determinants of Essential Oil Composition and Yield in Peppermint Leaves[1][W][OA]

Rigoberto Rios-Estepa[2], Iris Lange, James M. Lee, and B. Markus Lange*

Institute of Biological Chemistry (R.R.-E., I.L., B.M.L.), School of Chemical Engineering and Bioengineering (R.R.-E., J.M.L.), and M.J. Murdock Metabolomics Laboratory (B.M.L.), Washington State University, Pullman, Washington 99164–6340

We have previously reported the use of a combination of computational simulations and targeted experiments to build a first generation mathematical model of peppermint (*Mentha* × *piperita*) essential oil biosynthesis. Here, we report on the expansion of this approach to identify the key factors controlling monoterpenoid essential oil biosynthesis under adverse environmental conditions. We also investigated determinants of essential oil biosynthesis in transgenic peppermint lines with modulated essential oil profiles. A computational perturbation analysis, which was implemented to identify the variables that exert prominent control over the outputs of the model, indicated that the essential oil composition should be highly dependent on certain biosynthetic enzyme concentrations [(+)-pulegone reductase and (+)-menthofuran synthase], whereas oil yield should be particularly sensitive to the density and/or distribution of leaf glandular trichomes, the specialized anatomical structures responsible for the synthesis and storage of essential oils. A microscopic evaluation of leaf surfaces demonstrated that the final mature size of glandular trichomes was the same across all experiments. However, as predicted by the perturbation analysis, differences in the size distribution and the total number of glandular trichomes strongly correlated with differences in monoterpenoid essential oil yield. Building on various experimental data sets, appropriate mathematical functions were selected to approximate the dynamics of glandular trichome distribution/density and enzyme concentrations in our kinetic model. Based on a χ^2 statistical analysis, simulated and measured essential oil profiles were in very good agreement, indicating that modeling is a valuable tool for guiding metabolic engineering efforts aimed at improving essential oil quality and quantity.

The essential oil distilled from peppermint (*Mentha* × *piperita*) leaves is used in numerous consumer products (e.g. chewing gum, toothpaste, and mouthwash), as a flavor in the confectionary and pharmaceutical industries, and as a source of active ingredients for aromatherapy. Peppermint oil consists primarily of *p*-menthane-type monoterpenes, with smaller amounts of other monoterpenes and very minor quantities of sesquiterpenes (Rohloff, 1999). The essential oil is synthesized and accumulated in specialized anatomical structures called peltate glandular trichomes (Gershenzon et al., 1989; McCaskill et al., 1992). These trichomes contain secretory cells, arranged in an eight-celled disc, which are responsible for the synthesis of the oil. Nascent essential oil is secreted into an emerging cavity formed by the separation of a preformed layer of cuticular material (Amelunxen, 1965). Over the last two decades, the entire complement of genes and enzymes involved in the peppermint monoterpenoid essential oil biosynthetic pathway has been characterized (for review, see Croteau et al., 2005).

Transgenic peppermint plants have been generated in efforts aimed at modulating essential oil yield and composition. Mahmoud and Croteau (2001) reported that, by overexpressing the gene encoding 1-deoxy-D-xylulose 5-phosphate reductoisomerase (DXR), oil yield increases (compared with wild-type plants) of up to 50% were observed. Antisense suppression of the (+)-menthofuran synthase (MFS) gene led to a dramatic decrease in the amounts of the undesirable side product (+)-menthofuran (elite transgenic line designated MFS7a; Mahmoud and Croteau, 2001). A slight increase in overall monoterpene yields was reported for transgenic plants with increased expression levels of the gene encoding (−)-limonene syn-

[1] This work was supported by the mint commissions of the states of Washington, Oregon, Montana, and the Midwest United States, by the Agricultural Research Center at Washington State University, and by the U.S. Department of Energy (grant no. DE–FG02–09ER16054).

[2] Present address: Department of Chemical Engineering, Universidad de Antioquia, Medellin, 050010, Colombia.

* Corresponding author; e-mail lange-m@wsu.edu.

The author responsible for distribution of materials integral to the findings presented in this article in accordance with the policy described in the Instructions for Authors (www.plantphysiol.org) is: B. Markus Lange (lange-m@wsu.edu).

[W] The online version of this article contains Web-only data.

[OA] Open Access articles can be viewed online without a subscription.

www.plantphysiol.org/cgi/doi/10.1104/pp.109.152256

thase (LS; Diemer et al., 2001), whereas only negligible effects on yield were detected in an independent study (Krasnyansky et al., 1999). Transgenic plants overexpressing the gene coding for (−)-limonene 3-hydroxylase (L3H) did not accumulate increased levels of the recombinant protein, and the composition and yield of the essential oils were the same as in wild-type controls; however, cosuppression of the L3H gene resulted in a vastly increased accumulation of the intermediate (−)-limonene, without notable effects on oil yield (elite transgenic line designed L3H20; Mahmoud et al., 2004).

Mathematical modeling can be a powerful tool to support metabolic engineering efforts, including those performed with peppermint. Stoichiometric modeling only requires knowledge of the topology of reactions in the pathway and inputs/outputs. This is a particularly useful approach to determine flux distributions and the systemic characteristics of metabolic networks (for review, see Llaneras and Picó, 2008). When experimental designs supporting metabolic and isotopic steady state are employed, isotope labeling data can be utilized for the development of quantitative flux maps of metabolic pathways (for review, see Libourel and Shachar-Hill, 2008). For dynamic systems, kinetic modeling is regarded as the generally most suitable method (McNeil et al., 2000; Poolman et al., 2004; Bruggeman and Westerhoff, 2006; Rios-Estepa and Lange, 2007; Mendes et al., 2009). Building on the rich body of published data on the enzymology and physiology of the peppermint monoterpene pathway (for review, see Croteau et al., 2005), we recently developed a first generation kinetic model to simulate the dynamics of peppermint monoterpene composition (Rios-Estepa et al., 2008). Modeling indicated that the monoterpene profiles observed in leaves of plants grown under low-light conditions could be explained if one assumed that (+)-menthofuran, a dead-end side product, acted as a heretofore unknown competitive inhibitor against (+)-pulegone, the primary substrate of the branch point enzyme (+)-pulegone reductase (PR; Fig. 1). Follow-up biochemical studies established that this prediction was correct (Rios-Estepa et al., 2008), thus illustrating the utility of an approach that integrates mathematical modeling with experimental testing.

As part of this study, a computational perturbation analysis was used to predict factors with the potentially greatest impacts on peppermint essential oil yield and composition (specific biosynthetic enzymes and the density of oil-synthesizing trichomes). To test these modeling predictions experimentally, we first acquired biometric data with peppermint plants grown under several environmental conditions known to adversely affect oil accumulation (Burbott and Loomis, 1967; Clark and Menary, 1980) and the transgenic line MFS7a, for which an altered essential oil profile had been reported earlier (Mahmoud and Croteau, 2001). Building on these experimental data sets, we then developed a second generation model that accounts for biochemical, developmental, environmental, and genotypic factors of essential oil formation. This updated model was then used to simulate monoterpenoid essential oil profiles for the transgenic line MFS7a grown under low-light environmental stress conditions and the transgenic line L3H20, which had previously been shown to have vastly reduced expression levels of the gene encoding L3H. In both cases, simulated and measured monoterpene patterns were very similar, indicating that mathematical modeling has great potential for guiding efforts aimed at developing peppermint lines with high oil yields and favorable composition, even under adverse environmental conditions.

RESULTS

Experimental Design and Modeling Assumptions

As part of our ongoing efforts to expand our capabilities for utilizing mathematical modeling as a tool to generate testable hypotheses regarding the regulation of metabolic pathways, we evaluated the plasticity of peppermint monoterpenoid essential oil composition and yield under various environmental conditions and in two transgenic lines. In particular, we were interested in finding the minimum experimental data to support accurate simulations of monoterpene composition without any computational optimization of the model. This was possible because of the vast amount of available experimental data on the regulation of peppermint essential oil biosynthesis. All modeling assumptions were inferred directly from experimental observations, thus providing us with a unique opportunity to evaluate the depth of our understanding of this pathway. Here, we will provide a general overview of modifications to our first generation model (described in Rios-Estepa et al., 2008). A description of all modeling assumptions is given in Supplemental Data S1.

Expansion of Model Scope

Our first generation model was expanded by including reactions involved in the biosynthesis of terpenoid precursors (enzymes 1–9 in Fig. 1). The kinetic constants of enzymes, the rate equations reflecting enzyme properties, and all other parameters relevant to the current model are provided in Supplemental Data S1. A mechanism following regular Michaelis-Menten-type kinetics was assumed for all enzymes with the following exceptions: (1) reversible reaction mechanisms with appropriate equilibrium constants were introduced for DXR and (−)-menthone:(+)-neomenthol reductase (enzymes 2 and 18a, respectively, in Fig. 1; Davis et al., 2005; Rohdich et al., 2006); and (2) bi-bi reaction mechanisms (two substrates, two products) were assumed for 1-deoxy-D-xylulose-5-phosphate synthase (DXS; enzyme 1 in Fig. 1) and geranyl diphosphate synthase (enzyme 9 in Fig. 1). The former utilizes

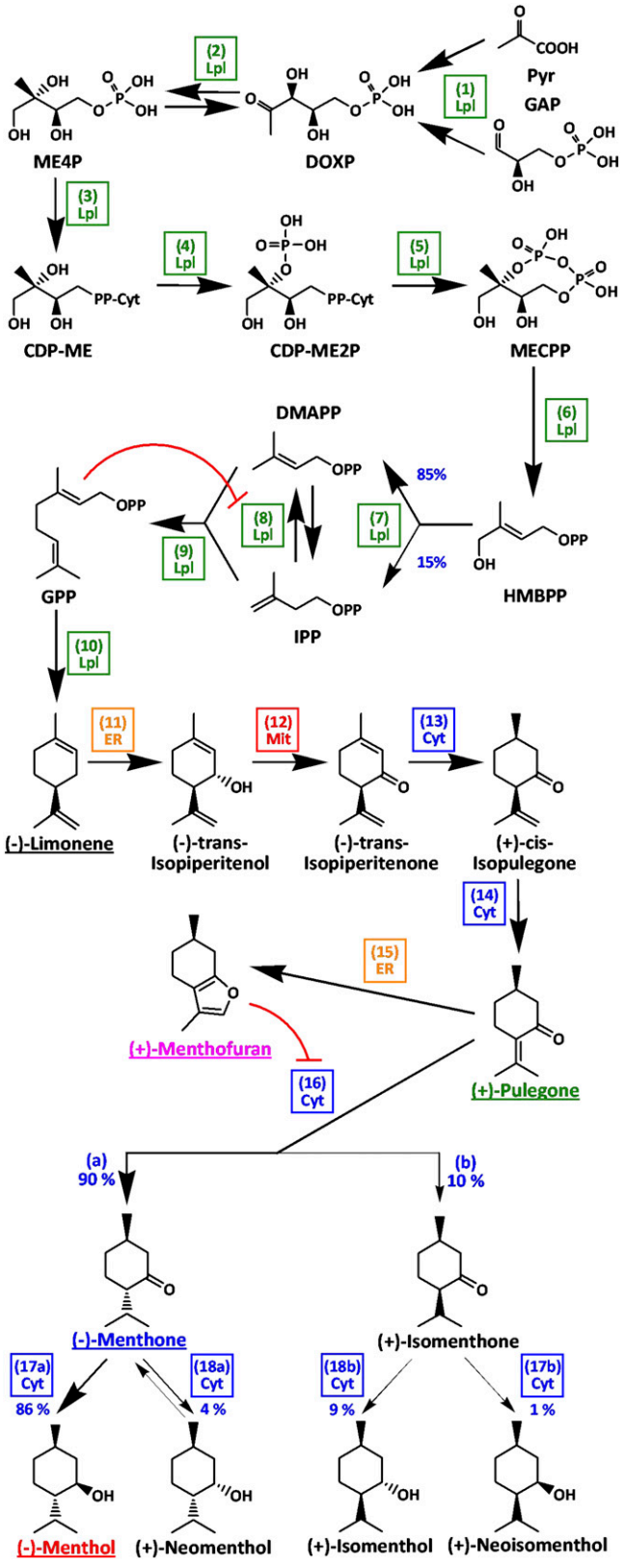

Figure 1. Outline of *p*-menthane monoterpene biosynthesis in peppermint glandular trichomes. The following enzymes are involved in this pathway: 1, 1-deoxy-D-xylulose 5-phosphate synthase; 2, 1-deoxy-D-xylulose 5-phosphate reductoisomerase; 3, 2C-methyl-D-erythritol 4-phosphate cytidyltransferase; 4, 4-(cytidine 5′-diphospho)-2C-methyl-D-erythritol kinase; 5, 2C-methyl-D-erythritol 2,4-cyclodiphosphate synthase; 6, (*E*)-4-hydroxy-3-methyl-but-2-enyl diphosphate synthase; 7, (*E*)-4-hydroxy-3-methyl-but-2-enyl diphosphate reductase; 8, isopentenyl diphosphate isomerase; 9, geranyl diphosphate synthase; 10, (−)-limonene synthase; 11, (−)-limonene 3-hydroxylase; 12, (−)-trans-isopiperitenol dehydrogenase; 13, (−)-trans-isopiperitenone reductase; 14, (+)-cis-isopulegone isomerase; 15, (+)-menthofuran synthase; 16a, (+)-pulegone reductase [(−)-menthone-forming activity]; 16b, (+)-pulegone reductase [(+)-isomenthone-forming activity]; 17a, (−)-menthone:(−)-menthol reductase [(−)-menthol-forming activity]; 17b, (−)-menthone:(−)-menthol reductase [(+)-neoisomenthol-forming activity]; 18a, (−)-menthone:(+)-neomenthol reductase [(+)-neomenthol-forming activity]; 18b, (−)-menthone:(+)-neomenthol reductase [(+)-isomenthol-forming activity]. The subcellular compartmentation of *p*-menthane metabolic enzymes is color coded as follows: Cyt (blue), cytosol; ER (orange), endoplasmic reticulum; Lpl (green), leucoplasts; Mit (red), mitochondria. The inhibitory effects of (+)-menthofuran on (+)-pulegone reductase and geranyl diphosphate on isopentenyl diphosphate isomerase are indicated by red arcs with orthogonal red lines. Names of selected metabolites are shown in the colors that are used to indicate the corresponding profiles in Figures 2 to 5.

an ordered mechanism (pyruvate binds first; Eubanks and Poulter, 2003), whereas a random mechanism was presumed for the latter.

Dynamic Simulation of Glandular Trichome Size and Distribution

Oil yield variation could potentially be caused by environment- and/or genotype-dependent differences in the size of glandular trichomes, which are responsible for synthesizing and storing essential oils. To evaluate this hypothesis and enable estimations of oil yield, trichomes were divided into three different size classes: large (75–82 μm diameter), medium (65–74 μm diameter), and small (50–65 μm diameter). The volume of the essential oil-filled subcuticular cavity of mature glandular trichomes was approximated by a sphere (volume: $^4/_3\,\pi\,r^3$, with r = radius) minus the volume of the secretory cells [$^1/_3\,\pi\,h\,(R^2 + R\,r + r^2)$, with R = radius at the wider end, r = radius at the narrower end, and h = height of the frustum], multiplied by an adjustment factor (0.9) to account for the fact that the oil storage cavity also contains nonoil mucilage (Supplemental Data S1). Trichome oil contents were thus estimated at 2.03×10^{-4} μL (large-sized trichomes), 1.40×10^{-4} μL (average-sized trichomes), or 0.66×10^{-4} μL (small-sized trichomes). It is also conceivable that the total number of glandular trichomes per leaf or the timing of glandular trichome formation could be modulated in plants with different oil yields. A logistic function to simulate experimentally determined glandular trichome distribution was selected based on manual trial-and-error experiments (Supplemental Data S1). This function specifies an initial lag time, then grows quickly and, because of limits in the size of the glandular trichome population, eventually levels off at the later stages of leaf development.

Approximation of Developmental Changes in Enzyme Concentrations

Enzyme concentrations are key parameters in kinetic models. The concentrations of monoterpene biosynthetic enzymes in leaf glandular trichomes of peppermint grown under greenhouse conditions had been inferred directly from experimental data (for details, see Rios-Estepa et al., 2008; Supplemental Data S1). However, it was not practically feasible to determine enzyme concentrations under various environmental conditions, at different stages of leaf development, and in different transgenic plants. Differences between greenhouse-grown wild-type plants and experimental plants were approximated by acquiring quantitative real-time PCR data for key biosynthetic genes and extrapolating differences in gene expression levels to changes in enzyme concentrations. Based on our experimental observations, a logarithmic function was introduced to approximate changes in enzyme levels from experimentally determined gene expression changes (Supplemental Data S1).

To assess gene expression patterns, secretory cells were isolated from leaves at 15 d after leaf emergence (the time of maximum essential oil biosynthetic activity), RNA was extracted (modified from Lange et al., 2000), and the expression levels of key genes involved in determining oil composition (PR and MFS; Fig. 2) and yield [DXS, DXR, 4-diphosphocytidyl-2C-methyl-D-erythritol kinase (CMK), 1-hydroxy-2-methyl-2-(*E*)-butenyl 4-diphosphate synthase (HDS), LS, and L3H] were assayed using quantitative real-time PCR. The "yield genes" were selected because the encoded enzymes are responsible for precursor supply and have relatively high K_m and low turnover number (K_{cat}) values. We used a Gauss function to approximate the shape of the curve representing temporal changes in gene expression levels based on extensive experimental data acquired with greenhouse-grown plants (Rios-Estepa et al., 2008; Supplemental Data S1).

Posttranslational Regulation of Pathway Flux

Feedback control was incorporated into our model by modifying appropriate rate equations based on experimental data: (1) substrate inhibition of PR (enzyme 16 in Fig. 1; Rios-Estepa et al., 2008); (2) competitive inhibition of PR by (+)-menthofuran (Rios-Estepa et al., 2008); and (3) competitive inhibition of isopentenyl-diphosphate isomerase (enzyme 8 in Fig. 1) by geranyl diphosphate (Ramos-Valdivia et al., 1997). In a recent publication (Rios-Estepa et al., 2008), we reported that the (+)-menthofuran concentration in secretory cells was roughly 400 μM when plants were grown under greenhouse conditions, which increased dramatically under low-light stress conditions. Since (+)-menthofuran is a competitive inhibitor of (+)-pulegone reductase, its concentration in secretory cells can have significant effects on oil composition and yield, which was accounted for by the introduction of the factor z (Supplemental Data S1). Analogously, the factor w was used to account for the amounts of the intermediate (+)-pulegone in secretory cells (Supplemental Data S1).

Testing the Validity of Modeling Assumptions

The focus of this study was to evaluate the minimum set of experimental data that, when incorporated into our model, generate simulations reflecting experimentally determined monoterpene profiles. It is important to note that we did not use any model-fitting approaches in this work. All modeling assumptions were inferred directly from experimental data. To assess the validity of our modeling assumptions, we performed a very basic goodness-of-fit analysis. We did not attempt to accurately simulate the entire time course of accumulation for each monoterpene. We were primarily interested in how well we could simulate the composition of monoterpenes at 40 d, which corresponds to the developmental stage when commercially grown peppermint would be harvested for oil extraction. From the χ^2 goodness-of-fit value for monoterpene profiles at 40 d (experimental versus simulated composition), we calculated a P value (Supplemental Data S1). In the context of our experiments, a nonsignificant P value ($P > 0.05$) means that there are no statistically significant differences between experimentally determined and simulated monoterpene composition at 40 d, indicating a good fit between experimental and simulated data.

Perturbation Analysis Identifies Key Factors Affecting Essential Oil Yield and Composition

To evaluate the role of individual enzyme activities in determining the composition of peppermint essential oil, we simulated monoterpene profiles by increasing or decreasing their concentrations in the model by 20%. These modifications of modeling parameters (perturbation analysis) were predicted to result only in relatively minor changes of oil yield (4% or less up or down), whereas notable correlations of specific enzyme activities with essential oil composition were predicted (Fig. 1). Modifications in the amounts of (−)-trans-isopiperitenol dehydrogenase (IsoDH; enzyme 12 in Fig. 1) were forecast to result in concomitant changes in the concentrations of (+)-menthofuran (up 36% when IsoDH is up 20%, and down 17% when IsoDH is down 20%; Fig. 2B). Modulation of PR concentration was predicted to be associated with changes in the concentrations of (+)-pulegone (59% down when PR is down 20%, and 40% up when PR is up 20%), (+)-menthofuran (25% up when PR is down, and 36% down when PR is up 20%), and (−)-menthone (12% up when PR is 20% up, and 70% down when PR is down; Fig. 2C). Differences in MFS concentration were predicted to impact primarily (+)-menthofuran concentrations (8% up when MFS is up 20%, and 7% down when MFS is down 20%;

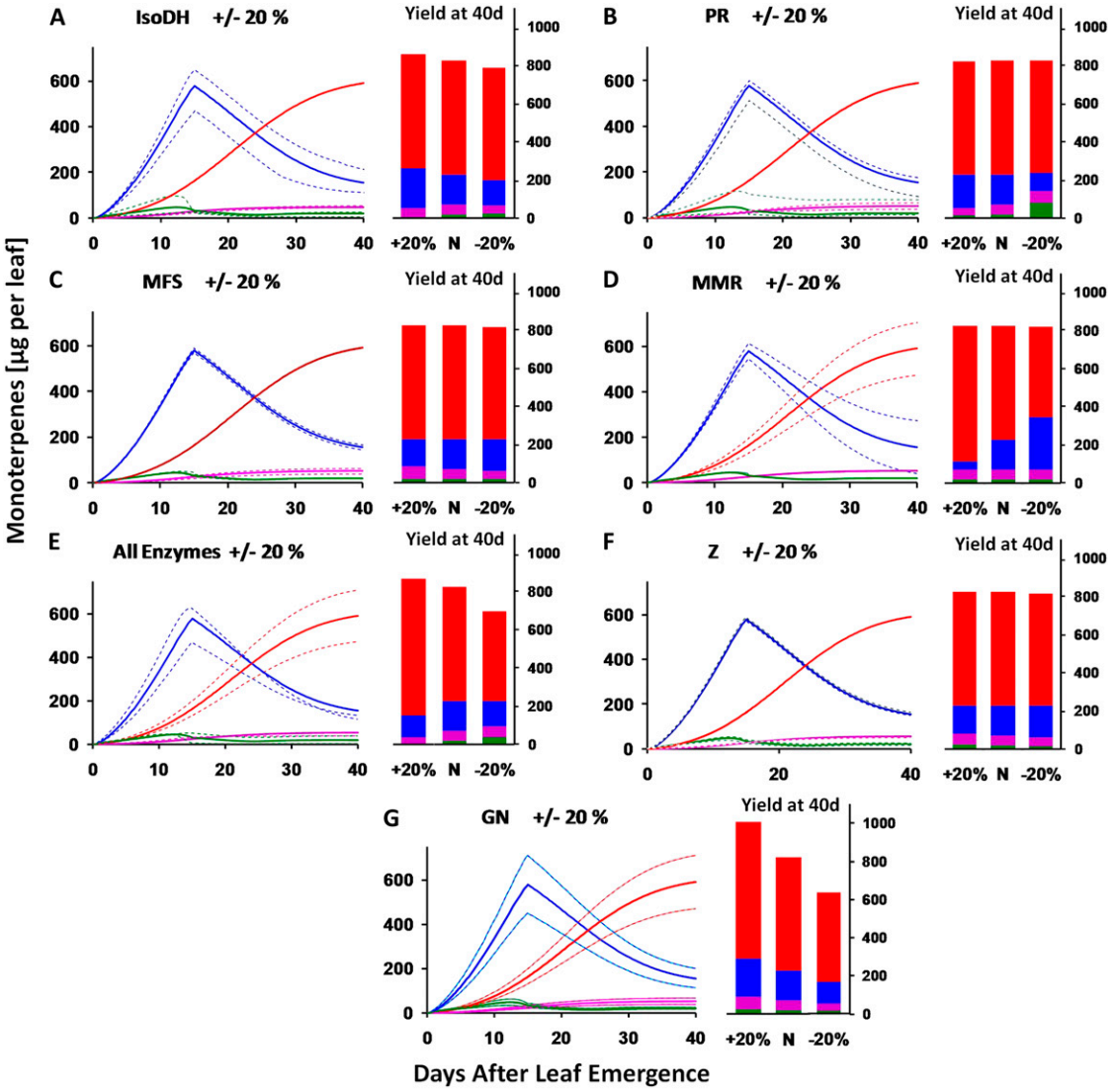

Figure 2. Perturbation analysis of monoterpenoid essential oil biosynthesis in peppermint predicts that glandular trichome density is a key factor controlling yield. The following colors are used for indicating monoterpene profiles: (+)-pulegone, green; (+)-menthofuran, pink; (−)-menthone, blue; (−)-menthol, red. A to E, The impact of changes in the abundance (±20% of regular greenhouse levels) of key proteins is indicated by broken lines for (−)-trans-isopiperitenol dehydrogenase (A), (+)-pulegone reductase (B), (+)-menthofuran synthase (C), (−)-menthone:(−)-menthol reductase (D), and all enzymes combined (E). F, The potential impact of variation in the amount of (+)-menthofuran retained in secretory cells under stress conditions (*z*-factor; for details, see Supplemental Data S1). G, Simulations of the potential effects of differences in the number of leaf glandular trichome monoterpene profiles. The bar graphs to the right of each panel indicate the amounts of (+)-pulegone, (+)-menthofuran, (−)-menthone, and (−)-menthol (from bottom to top) at 40 d after leaf emergence. N, Oil yield under normal greenhouse conditions.

Fig. 2D). As shown in Figure 2E, changes in the concentration of (−)-menthone:(−)-menthol reductase (MMR; enzyme 17a in Fig. 1) were modeled to affect the profiles of (−)-menthone (74% down when MMR is up 20%, and 76% up when MMR is down 20%) and (−)-menthol (19% up when MMR is up 20%, and 20% down when MMR is down 20%). When the concentrations of all enzymes considered in our model were raised by 20% (in a coordinated fashion), the model predicted a modest 5% increase in oil yield, whereas lowering all enzyme concentrations by 20% was modeled to result in a more pronounced oil yield decrease (15%; Fig. 2F). Modifications of the factor *z*, which accounts for the retention of (+)-menthofuran in secretory cells under adverse environmental conditions (Supplemental Data S1), were predicted to lead to only minor changes in oil yield (less than 1% change when *z* is 20% up or down) and composition (Fig. 2G). The strongest correlation between modulation of a potential yield factor and measured oil yields was observed

if one assumed an increase or decrease in the density of leaf glandular trichomes (22% up with 20% increased glandular trichome density, and 28% down with 20% decreased glandular trichome density; Fig. 2H). We thus performed a series of experiments to assess this prediction experimentally.

Simulation of the Essential Oil Profile in Transgenic Peppermint Line MFS7a

Experimental Design and Essential Oil Yields

We chose to reevaluate a transgenic line that had previously been demonstrated to produce monoterpene profiles that are significantly different from those of wild-type plants. This line, designated MFS7a, had been transformed with a construct containing an antisense cDNA of the peppermint (+)-menthofuran synthase gene (Mahmoud and Croteau, 2001) and was generated initially to reduce the levels of the undesirable dead-end pathway side product (+)-menthofuran. The MFS7a line, which accumulates the MFS transcript to only 14% of the levels in wild-type plants (Mahmoud and Croteau, 2001), has been propagated under greenhouse growth conditions for 7 years along with its wild-type progenitor. The MFS7a antisense plants accumulated, compared with wild-type plants, lower levels of both (+)-menthofuran (20% of the wild type) and (+)-pulegone (20% of the wild type; Fig. 3, A and B), and, surprisingly, produced 35% higher oil yields compared with the wild type (Fig. 3F).

Using Gene Expression Data to Approximate Enzyme Concentrations

The expression levels of the genes encoding DXS, DXR, CMK, HDS, LS, L3H, and MFS were higher in wild-type controls compared with MFS7a plants (4.0-, 1.4-, 1.4-, 2.4-, 4.4-, 2.9-, and 7.2-fold higher, respectively; Fig. 3E). In contrast, the PR gene was expressed at very low levels in the wild type (6.9-fold lower than in MFS7a plants). As described above, a function was used to approximate enzyme concentrations from these experimentally determined gene expression levels (Supplemental Data S1).

Glandular Trichome Dynamics

At 30 d after leaf emergence, the majority of glandular trichomes on wild-type leaves were of medium size (57%), with a substantial proportion (39%) of large-sized and a low proportion (4%) of small-sized trichomes (Fig. 3G). In contrast, the MFS7a line contained a substantially higher proportion of large-sized glandular trichomes (67% at 30 d), fewer medium-sized trichomes (33%), and no small trichomes (Fig. 3G). Leaves of greenhouse-grown plants at 30 d after emergence contained an average of 10,151 glandular trichomes, which is very similar to the estimate used thus far (10,000 trichomes per leaf). At 30 d, MFS7a plants contained an average of 12,382 glandular trichomes per leaf, about 22% higher than in the wild type. When both the size distribution and the density of glandular trichomes were taken into account, the total monoterpene yield at 30 d was calculated to be 1,477 μg per leaf for wild-type plants (Fig. 3F), which is only 3.8% off the measured value (1,535 $\pm$ 156 μg per leaf). Using the same approach, total monoterpene content in MFS7a plants was estimated to be 2,028 μg per leaf (2.5% off the measured value of 2,079 $\pm$ 155 μg per leaf; Fig. 3F). These calculated monoterpene contents were about 37% higher in MFS7a than in the wild type, which was very close to the experimentally determined yield difference (35%).

Modeling Results

To evaluate if a combination of gene expression patterns and glandular trichome density and size distribution could account for both monoterpene composition and yield in wild-type plants grown in the greenhouse (WT-GH) and transgenic MFS7a plants grown in the greenhouse (MFS7a-GH) plants under different environmental conditions, we modified our kinetic mathematical model for peppermint essential oil biosynthesis with the experimental data obtained as part of this study (estimated enzyme levels based on measured gene expression patterns [Fig. 3D] and experimentally determined trichome distribution and density [Fig. 3, E and F]). In comparison with WT-GH plants (Fig. 3A), MFS7a-GH plants were forecast to have high oil yields and a favorable composition [high levels of (−)-menthol, with very low levels of (+)-pulegone and (+)-menthofuran; Fig. 3B]. Based on a χ^2 analysis, the P values for the comparisons of simulated versus experimental data were 0.6123 (WT-GH) and 0.1756 (MFS7a-GH; Fig. 3C), indicating that the simulated monoterpene composition was not statistically different from measured data (good fit).

Simulation of the Effects of Environmental Stress Conditions on Essential Oil Profiles

Experimental Design and Essential Oil Yields

It has been known that, when peppermint plants are grown at low-light intensities, water deficit, or high night temperatures, poor quality oils with elevated amounts of the undesirable metabolites (+)-pulegone and (+)-menthofuran are produced with concomitant decreases in oil yield (Burbott and Loomis, 1967; Clark and Menary, 1980). To reproduce such environmental conditions, WT-GH control plants, wild-type plants under water deficit (50% of regular volume of fertilizer mix; designated WT-LW), wild-type plants at decreased light intensity (roughly 30% of regular photon flux; designated WT-LL), or wild-type plants under conditions with a combination of low light intensities (as above) and high night temperatures (constant day and night temperatures at 30°C; designated WT-LL/HT)

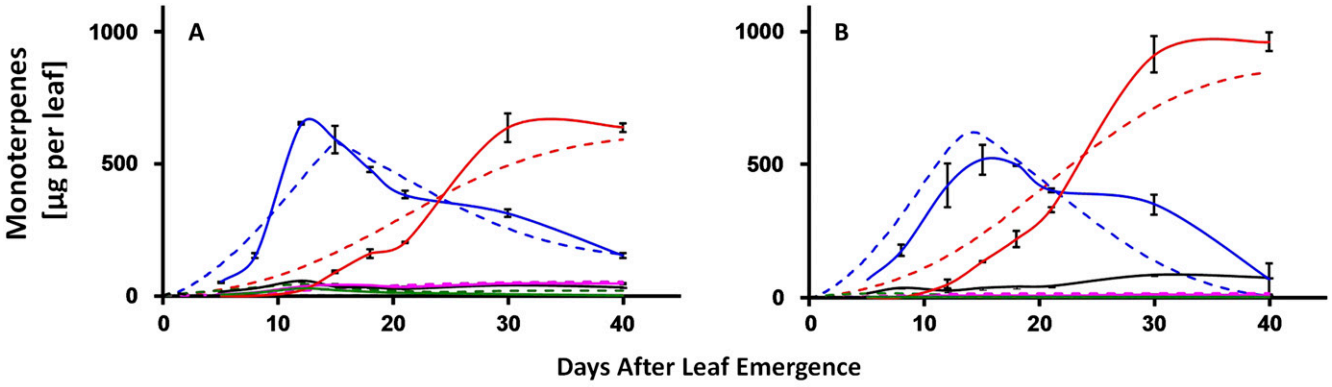

C

Plant Line/ Treatment	Data Type	Monoterpene Composition [% of Total p-Menthane Monoterpenes ± Strd. Error] (-)-Limonene	(-)-Menthone	(+)-Menthofuran	(-)-Menthol	(+)-Pulegone	Other	Chi Square Value	P-Value
WT-GH	Experimental	3.14 ± 0.18	14.43 ± 0.84	4.35 ± 0.15	60.47 ± 1.57	0.11 ± 0.08	17.50 ± 1.38		
	Model	0.01	16.07	5.37	61.01	0.06	17.48	3.5731661	0.6123 (N.S.)
MFS7a-GH	Experimental	5.48 ± 0.06	5.17 ± 2.39	0.70 ±0.06	71.18 ± 2.57	0.01 ± 0.007	17.47 ± 0.08		
	Model	0.85	1.68	1.33	75.51	0.01	20.62	7.6661367	0.1756 (N.S.)

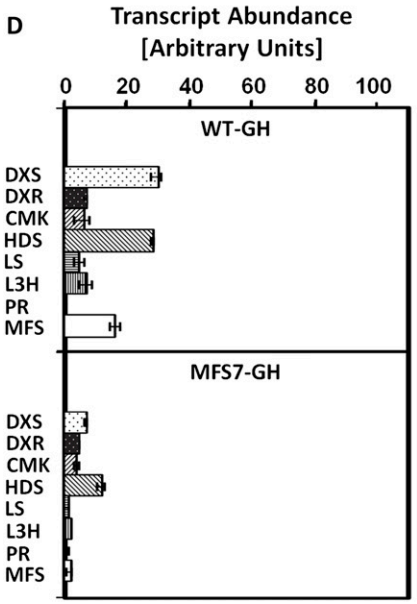

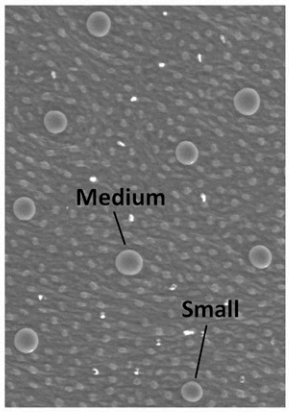

F

Glandular Trichomes: Size Distribution	[%]	Density [per leaf]	Monoterpene Yield: Calculated [µg per leaf]	Experimental [µg per leaf]
WT-GH				
Large	39	3959	722	
Medium	57	5786	731	
Small	4	406	24	
Total		10151	1477	1535 ± 156
MFS7a-GH				
Large	67	8296	1512	
Medium	33	4086	516	
Small	0	0	0	
Total		12382	2028	2079 ± 155

Figure 3. A and B, Comparisons of experimentally determined and simulated monoterpene profiles of WT-GH (A) and MFS7a-GH (B) plants (experimental data with error bars [n = 3]; simulations as broken lines). For color coding of lines representing individual metabolites, see Figure 2. C, The χ^2 statistical analysis of goodness of fit at 40 d after leaf emergence. N.S., Not significant (indication of good fit). D, Expression patterns of genes involved in peppermint monoterpene biosynthesis at 15 d after leaf emergence, as determined by real-time quantitative PCR (n = 3), using the peppermint β-actin gene (AW255057) as an endogenous control. The average signal intensity of RNA obtained with 30-d samples (wild-type plants grown under greenhouse conditions) was used as a calibrator (based on prior knowledge that expression levels of genes involved in monoterpene biosynthesis are consistently low [but detectable] at this stage of leaf development). E, Microscopic image of the surface of a peppermint leaf. F, Data on glandular trichome density and size distribution (n = 5) as well as total essential oil yield at 30 d after leaf emergence (n = 3).

were used. As expected, the oil yield decreased under stress conditions (compared with WT-GH controls, oil yields were 1.6-, 2.3-, and 4.1-fold lower in WT-LW, WT-LL, and WT-LL/HT plants, respectively; Fig. 4F). In WT-LW plants, the profiles of the major monoterpenes changed only slightly, and the major difference from WT-GH plants was a 36.5% reduction in oil yield (Fig. 4A). In WT-LL plants, the amount of the inter-

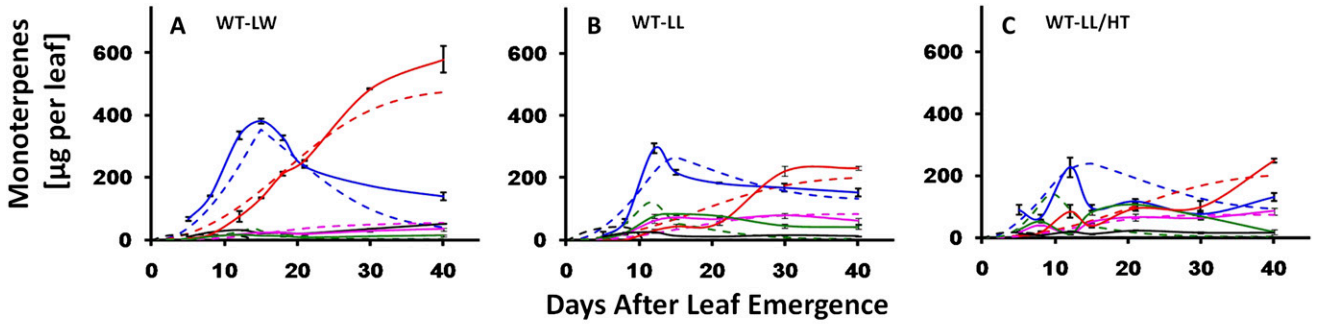

D

Plant Line/ Treatment	Data Type	Monoterpene Composition [% of Total p-Menthane Monoterpenes ± Strd. Error] (-)-Limonene	(-)-Menthone	(+)-Menthofuran	(-)-Menthol	(+)-Pulegone	Other	Chi Square Value	P-Value
WT-LW	Experimental	5.43 ± 0.60	14.56 ± 1.43	3.50 ± 0.36	60.40 ± 4.48	1.36 ± 0.38	14.75 ± 0.87		
	Model	0.82	10.3	5.05	66.5	1.37	15.96	6.5620544	0.2553 (N.S.)
WT-LL	Experimental	2.04 ± 0.24	26.38 ± 1.26	10.40 ± 0.45	39.90 ± 2.96	7.06 ± 0.38	14.22 ± 2.16		
	Model	0.09	26.42	16.56	40.23	2.46	14.24	8.5125712	0.1302 (N.S.)
WT-LL/HT	Experimental	2.77 ± 0.09	22.56 ± 2.09	14.69 ± 1.85	42.68 ± 0.99	3.08 ± 1.26	14.22 ± 1.96		
	Model	0.88	24.98	13.75	36.92	7.97	15.5	10.265553	0.0682 (N.S.)

E

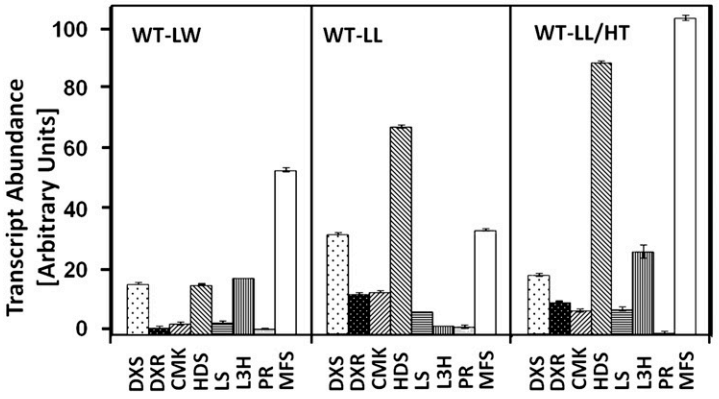

F

	Glandular Trichomes Size Distribution [%]	Glandular Trichomes Density [per leaf]	Monoterpene Yield Calculated [µg per leaf]	Monoterpene Yield Experimental [µg per leaf]
WT-LW				
Large	44	3200	583	
Medium	53	3855	487	
Small	3	218	13	
Total		7273	1083	974 ± 51
WT-LL				
Large	40	2802	511	
Medium	56	3922	496	
Small	4	280	17	
Total		7004	1023	658 ± 73
WT-LL/HT				
Large	7	351	64	
Medium	49	2458	311	
Small	44	2207	131	
Total		5017	505	377 ± 9

Figure 4. A to C, Comparisons of experimentally determined and simulated monoterpene profiles of wild-type plants grown under various stress conditions: low water (A), low light intensity (B), and low light intensity and high night temperatures (C; experimental data with error bars [n = 3]; simulations as broken lines). For color coding of lines representing individual metabolites, see Figure 2. D, The χ^2 statistical analysis of goodness of fit at 40 d after leaf emergence. N.S., Not significant (indication of good fit). E, Expression patterns of genes involved in peppermint monoterpene biosynthesis at 15 d after leaf emergence (n = 3). F, Data on glandular trichome density and size distribution (n = 5) as well as total essential oil yield at 30 d after leaf emergence (n = 3).

mediate (+)-pulegone increased transiently to 82 μg per leaf (4.1-fold higher than in WT-GH controls), whereas the (+)-menthofuran content increased linearly to 77 μg per leaf at 30 d (70% higher than in WT-GH controls), with a concomitant decrease in total oil yield (Fig. 4B). When low-light stress was combined with high night temperatures (WT-LL/HT), the amount of the intermediate (+)-pulegone increased transiently to 105 μg per leaf (5.3-fold higher than in WT-GH controls) and the (+)-menthofuran content increased linearly to 63 μg per leaf at 30 d (40% higher than in WT-GH controls; Fig. 4C). The z value, which accounts for the selective retention of (+)-menthofuran in secretory cells under stress conditions, was adjusted accordingly (Supplemental Data S1).

Using Gene Expression Data to Approximate Enzyme Concentrations

In comparison with WT-GH controls, gene expression levels of DXS, DXR, CMK, HDS, and LS decreased in WT-LW samples, whereas transcript abundance of

these genes increased in WT-LL and WT-LL/HT plants (Fig. 4E). Compared with WT-GH, L3H transcript levels were lower in WT-LL (2.5-fold down) and higher in WT-LW and WT-LL/HT samples (2.6- and 3.9-fold up, respectively). The expression levels of the gene encoding PR increased slightly under all stress conditions, whereas MFS expression was notably induced in WT-LL and WT-LL/HT (6.3- and 3.3-fold up, respectively; Fig. 4E). These results were used to approximate environment-dependent changes in the corresponding enzyme concentrations and introduced as parameters in our kinetic model (Supplemental Data S1).

Glandular Trichome Dynamics

Glandular trichome density was substantially lower on leaves of plants grown under adverse environmental conditions (7,273, 7,004, and 5,014 glandular trichomes per leaf for WT-LW, WT-LL, and WT-LL/HT plants, respectively; Fig. 4F). The distribution of different sized glandular trichomes was similar in WT-GH, WT-LW, and WT-LL plants. However, at 30 d after leaf emergence, plants grown under severe stress conditions (WT-LL/HT) had a substantially higher proportion of small-size trichomes at the expense of large-sized trichomes. Plants grown under water deficit conditions (WT-LW) produced 974 $\pm$ 51 μg of total monoterpenes per leaf, corresponding to a 60% decrease compared with greenhouse-grown controls. When peppermint plants were grown under low light intensities (WT-LL), the essential oil yield (658 $\pm$ 73 μg of monoterpenes per leaf) was roughly 2.3-fold lower than in WT-GH controls. Under severe stress conditions (WT-LL/HT), the measured essential oil yield was even lower at 377 $\pm$ 9 μg of monoterpenes per leaf. Based on these measurements, we adjusted the logistic function used to account for the developmental and environmental dynamics of trichome density in our mathematical model.

Modeling Results

The simulated and experimentally determined monoterpene profiles were qualitatively very similar for WT-LW and WT-LL plants, whereas the temporal changes of monoterpene levels in WT-LL/HT plants were quite complex (Fig. 4, A–C). Based on a χ^2 statistical analysis, the simulated monoterpene composition [in particular, high accumulation levels of (+)-menthofuran under LL and LL/HT conditions] was in good agreement with experimental values (nonsignificant P values of 0.2553, 0.1302, and 0.0682 for WT-LW, WT-LL, and WT-LL/HT, respectively). Not unexpectedly, the goodness of fit between simulated and measured data decreased with increasing severity of stress caused by growth conditions.

Simulation of Monoterpene Profiles Based on Minimal Experimental Data

First Case Study

To further evaluate the utility of our kinetic mathematical model, we assessed the minimum set of experimental data needed to accurately simulate experimental outcomes. As a first test case, we modeled monoterpene profiles of transgenic MFS7a plants (antisense-based reduction of MFS transcript levels) grown under low-light conditions (MFS7a-LL) based on two experimental data sets. First, we determined the total monoterpene yield as 1,113 $\pm$ 115 μg per leaf (Fig. 5E). Based on previous measurements, we estimated that this yield would translate into roughly 7,500 glandular trichomes (this turned out to be a good estimate, as we later counted 8,262 glandular trichomes per leaf of MFS7a-LL plants; Fig. 5E). We had also determined previously that, in WT-LL plants, (+)-menthofuran accumulated preferentially in secretory cells, thus leading to an inhibition of PR activity (Rios-Estepa et al., 2008). Assuming analogous dynamics for MFS7a-LL, the z factor to account for the retention of (+)-menthofuran in secretory cells was adjusted (Supplemental Data S1). We used quantitative real-time PCR to acquire expression data for key genes involved in peppermint monoterpene biosynthesis (Fig. 5C). These were then used to estimate enzyme concentrations in the Michaelis-Menten rate equations of the model (Supplemental Data S1). After these adjustments, a computational simulation predicted qualitatively lower monoterpene yields compared with MFS7a-GH (the same genotype grown under ideal conditions) but substantially higher yields than in the low-light-grown wild-type plants (WT-LL; Fig. 5A). In particular, the amounts of the desirable monoterpenes (−)-menthone and (−)-menthol were simulated to be higher in MFS7a-LL than in WT-LL, whereas the undesirable oil components (+)-pulegone and (+)-menthofuran were lower. The simulated monoterpene composition at 40 d was in good agreement with experimental data, as indicated by a nonsignificant P value of 0.1694 (Fig. 5C).

Second Case Study

As a second test case, we predicted monoterpene accumulation patterns of transgenic L3H20 plants (cosuppression-based reduction of L3H) grown under greenhouse conditions (L3H20-GH), utilizing even fewer experimental data than in the first test case. The L3H expression levels in L3H20 had previously been determined to be less than 0.1% of those in wild-type plants (Mahmoud et al., 2004). We assumed that this was the only gene affected in this transgenic line and changed the maximum enzyme concentration of L3H in our mathematical model (but not any other enzyme level; Fig. 5F). Using these assumptions, the model predicted high (−)-limonene levels at approx-

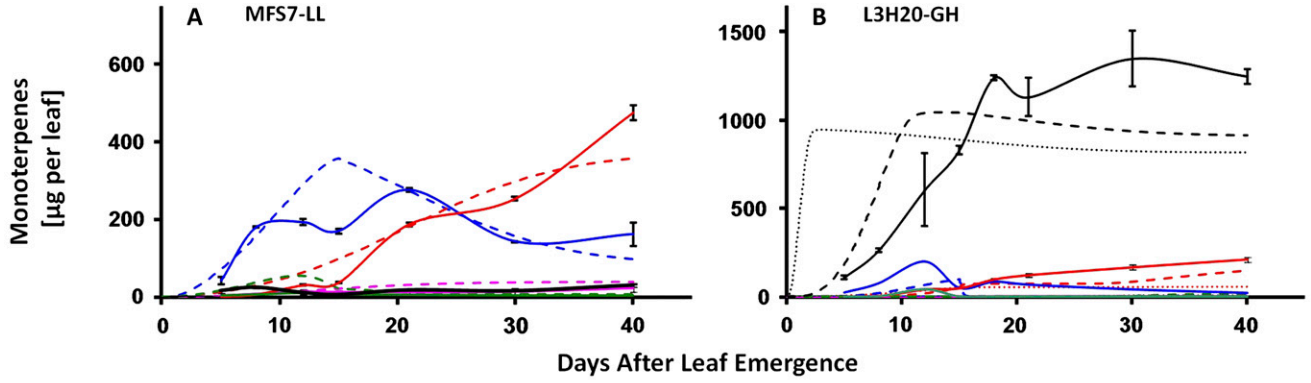

C

Plant Line/ Treatment	Data Type	Monoterpene Composition [% of Total p-Menthane Monoterpenes ± Strd. Error] (-)-Limonene	(-)-Menthone	(+)-Menthofuran	(-)-Menthol	(+)-Pulegone	Other	Chi Square Value	P-Value
MFS7a-LL	Experimental	3.03 ± 0.37	16.21 ± 3.46	2.39 ± 0.46	47.35 ± 8.67	0.21 ± 0.03	30.9 ± 2.75		
	Model	0.97	14.36	5.67	53.14	0.06	25.8	7.7699825	0.1694 (N.S.)
L3H-GH	Experimental	82.13 ± 2.61	1.52 ± 0.09	0.18 ± 0.01	13.88 ± 0.87	0.07	2.29 ± 0.25		
	Model 1	89.23	0.01	0.5	6.15	0.45	3.66	8.3866536	0.1362 (N.S.)
	Model 2	82	0.54	0.67	13.4	0.48	2.91	3.7572774	0.5849 (N.S.)

D

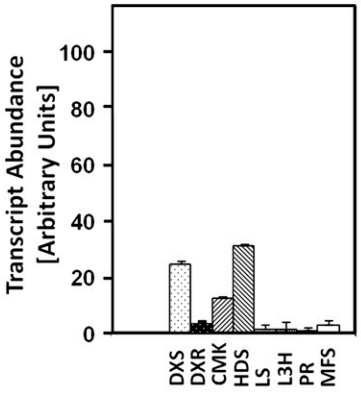

E

Glandular Trichomes Size Distribution	[%]	Density [per leaf]	Monoterpene Yield Calculated [µg per leaf]	Experimental [µg per leaf]
MFS7a-LL				
Large	51	4214	768	
Medium	44	3635	459	
Small	5	413	24	
Total		8262	1252	1113 ± 115
L3H20-GH				
Large	41	4463	813	
Medium	49	5334	674	
Small	10	1089	64	
Total		10885	1552	1686 ± 58

F Modeling Assumptions:

MFS7-LL (A)
- Essential oil yield (exp.)
- Transcript patterns (exp.)
- Increased z-value (Rios-Estepa et al., 2008)

L3H20-GH (B1)
- Essential oil yield (exp.)
- Reduction of L3H expression (Mahmoud and Croteau, 2001)

L3H20-GH (B2)
- Assumptions as above plus: Delayed glandular trichome development (exp.)

Figure 5. A and B, Comparisons of experimentally determined and simulated monoterpene profiles of transgenic lines MFS7a-LL (A) and L3H20-GH (B [dotted lines, model 1; broken lines, model 2]). For color coding of lines representing individual metabolites, see Figure 2. C, The χ^2 statistical analysis of goodness of fit at 40 d after leaf emergence. N.S., Not significant (indication of good fit). D, Expression patterns of genes involved in peppermint monoterpene biosynthesis at 15 d after leaf emergence ($n = 3$). E, Data on glandular trichome density and size distribution ($n = 5$) as well as total essential oil yield at 30 d after leaf emergence ($n = 3$). F, Simulations were performed based on modeling assumptions that were inferred from minimal experimental data taken from the literature (references given) or acquired as part of this study (exp.).

imately 850 μg per leaf and low (−)-menthol levels (approximately 60 μg per leaf), whereas no other metabolite should accumulate to appreciable levels (Fig. 5B, dotted line). The simulated monoterpene composition, which was based on only one previously published experimental measurement (down-regulation of L3H expression; Mahmoud et al., 2004), was very similar to the experimentally determined data (non-significant P value of 0.1362; Fig. 5C). However, the simulated profiles differed from the measured patterns by a much sharper increase in (−)-limonene levels as opposed to the slower accumulation detected experimentally (Fig. 5B).

To assess the cause of this discrepancy, we measured essential oil yields and evaluated glandular trichome distribution patterns in L3H20-GH plants. The total oil yield at 30 d was determined as 1,686 ± 58 μg per leaf, which is slightly higher than the WT-GH oil content (1,535 ± 156 μg per leaf). The trichome distribution, however, was notably different. Glandular trichomes on L3H20-GH plants appeared to mature slower than those on WT-GH plants, as indicated by the size distribution (L3H20-GH, 41% large, 49% medium, 10% small [Fig. 5F]; WT-GH, 39% large, 57% medium, 4% small [Fig. 3F]). Thus, for a second modeling attempt, the logistic function used to account for

developmental dynamics in glandular trichome distribution was adjusted to reflect a delayed onset of the exponential growth phase (Supplemental Data S1). It was also assumed that, because of the retarded trichome maturation in L3H20-GH, enzyme profiles would be shifted by reaching their maximum 5 d later (at 20 d) than in WT-GH. Based on these updated assumptions (model 2), the simulation predicted a slower increase in (−)-limonene levels and slightly higher (−)-menthol levels (Fig. 5B, dashed line). The simulated monoterpene composition was in good agreement with measured data (nonsignificant *P* value of 0.5849).

DISCUSSION

Biosynthetic Gene Expression Patterns Correlate with Monoterpenoid Essential Oil Composition But Not with Yield

Probably the most obvious variables with potential effects on monoterpenoid essential oil composition and yield are biosynthetically relevant gene expression levels and enzyme activities. Interestingly, mRNA levels of DXS, DXR, CMK, HDS, LS, L3H, and MFS were lower in MFS7a plants compared with wild-type controls at the peak of oil biosynthesis, despite a 35% higher oil yield of the transgenic line (Fig. 3, D and F). In contrast, the decreased amounts of (+)-pulegone and (+)-menthofuran in MFS7a-GH plants (compared with WT-GH) were indeed reflected in the expression levels of the biosynthetic genes (low MFS and high PR expression levels). The expression levels of genes with potential impact on yield (DXS, DXR, CMK, HDS, LS, and L3H) in plants grown under various adverse environmental conditions (WT-LW, WT-LL, and WT-LL/HT) were similar to those in WT-GH, although significantly decreased oil yields were detected in stressed plants. In contrast, expression levels of genes related to essential oil composition (PR and MFS) correlated well with oil yields across all environmental conditions. Taken together, gene expression patterns appeared to be consistent with monoterpene composition, but not yield, in both wild-type and MFS7a plants.

To further evaluate the potential effects of enzyme concentrations on metabolite profiles, we performed a perturbation analysis. This analysis indicated that several enzymes (IsoDH, PR, MFS, and MMR) should have significant control over oil composition. Based on our experimental data, the most relevant changes observed under various environmental conditions were modulations of the concentrations of (+)-pulegone and (+)-menthofuran (Figs. 3–5), which were suggested (by way of perturbation analysis) to be primarily due to changes in the levels of PR and/or MFS (Fig. 2). In contrast, oil yield was affected only slightly when individual enzyme concentrations in the model were increased or decreased by 20% (Fig. 2). These modeling results indicated that key enzyme activities are unlikely to be major determinants of oil yield. Such a conclusion is in agreement with the flux-control summation theorem of metabolic control analysis, which states that all enzymes share control over pathway flux, albeit to different degrees (Kacser and Burns, 1973; Heinrich and Rapoport, 1974). When the concentrations of all enzymes directly relevant to monoterpene biosynthesis in peppermint were modified in the model (coordinately up or down by 20%), the yield was affected by 5% (up) or 17% (down; Fig. 2). This means that, although enzyme concentrations can have notable effects on oil yield, other factors must be taken into account to explain the magnitude of changes observed experimentally (e.g. 35% yield increase in MFS7a-GH plants and 75% yield decrease in WT-LL/HT plants, both compared with WT-GH plants).

Maximum Glandular Trichome Size Is Constant But Size Distribution and Density Can Vary Substantially

One possible explanation for high oil yields in MFS7a plants (compared with the wild type) would be a higher import of carbohydrates from photosynthetic cells into nonphotosynthetic glandular trichomes, thus resulting in larger precursor pools and a potentially higher oil synthesis in each trichome. This would mean that the volume of the cavity holding the essential oil would be larger. To test the hypothesis that trichomes might synthesize increased amounts of essential oil, we measured the diameters of glandular trichomes on leaf surfaces of wild-type and MFS7a plants. Interestingly, the maximum diameter of glandular trichomes turned out to be constant (82 μm) and independent of genotype or environmental growth conditions (Figs. 3–5). However, we noticed that the distribution of trichomes of different sizes correlated with oil yield in a genotype- and environment-dependent fashion. For example, glandular trichomes on MFS7a plants emerged and matured earlier than those of wild-type plants, which was reflected in an increased proportion of large trichomes (75–82 μm diameter; 67% in MFS7a-GH versus 39% in WT-GH; Fig. 3F). The emergence and maturation of glandular trichomes on plants grown under certain adverse environmental conditions (WT-LW and WT-LL) were similar to those in WT-GH controls and did not correlate with oil yield (Fig. 4F). Only plants grown under severe stress conditions (WT-LL/HT) had a much higher percentage of small (50–65 μm diameter) trichomes (44% in WT-LL/HT versus 4% in WT-GH), in accordance with low oil yield (Fig. 4F). A gradient of glandular trichome sizes is generally regarded as an indicator of specific stages of leaf development (Turner et al., 2000). Thus, our results indicate that the architecture of peppermint glandular trichomes is a fixed parameter, whereas the program controlling trichome development is flexible. By combining the trichome distribution data with an estimate of 10,000 glandular

trichomes per leaf (Colson et al., 1993), one can approximate oil yields in MFS7a-GH and WT-GH plants (for details, see Supplemental Data S1). Based on these calculations, total monoterpene contents would be estimated to be very similar at 1,455 and 1,638 μg per leaf for WT-GH and MFS7a-GH plants, respectively (11% difference), whereas we detected a 35% difference experimentally (Fig. 3F). Using the same approach, oil yields for plants grown under adverse environmental conditions could be vastly overestimated (estimated versus experimental yields are as follows: WT-LW, 1,489 versus 974 $\pm$ 51 μg per leaf; WT-LL, 1,460 versus 658 $\pm$ 73 μg per leaf; WT-LL/HT, 1,007 versus 377 $\pm$ 9 μg per leaf), thus indicating that an additional factor needed to be considered for more accurate estimations.

While collecting glandular trichome distribution data, we also counted the number of glandular trichomes on leaves taken from wild-type and MFS7a plants grown under various environmental conditions. When these counts and trichome distribution data were combined, calculated oil yields for most samples deviated less than 12% from experimentally determined values (WT-GH, WT-GW, MFS7a-GH, MFS7a-LL, and L3H-GH). Larger discrepancies were observed only when plants were grown under severe stress conditions (WT-LL, estimate 36% too high; WT-LL/HT, estimate 25% too high). However, the oil yield trends (e.g. MFS7a-GH > WT-GH; MFS7a-LL > WT-LL; WT-GH > WT-LW > WT-LL > WT-LL/HT) were reflected in all approximations (Figs. 3–5).

What Are the Mechanisms Regulating Glandular Trichome Density and Size Distribution?

An important as yet unanswered question relates to the cause of differences in trichome densities and developmental distribution. The higher oil yields obtained from MFS7a plants are surprising, as the only major difference from the wild type at the transcriptional level is the reduced MFS transcript abundance. MFS expression levels should have effects on oil composition, but one might ask why we determined an increased number of leaf trichomes compared with the wild type. By the same token, it is entirely unknown which signals control the reduction of glandular trichome numbers under certain environmental stress conditions.

The plant hormone methyl jasmonate (MeJA) is known to induce various developmental and defense responses in plants. When applied to the stems of certain conifers, MeJA caused the formation of traumatic resin ducts, concomitant with an induction of terpenoid resin secretion (Martin et al., 2002; Hudgins et al., 2003, 2004). Spraying Arabidopsis (*Arabidopsis thaliana*) with MeJA led to the induced production of trichome hairs (nonglandular trichomes) on leaf surfaces (Traw and Bergelson, 2003; Yoshida et al., 2009). MeJA application also induced an increased number of terpenoid-emitting glandular trichomes on tomato (*Solanum lycopersicum*) leaves (Boughton et al., 2005; van Schie et al., 2007). It is conceivable that variation in trichome density and distribution on mint leaves is controlled by the same, or at least similar, regulatory processes. In the context of the experiments reported here, it will be highly informative to test the possible existence of a "push-pull" mechanism (increased expression of a biosynthetic gene induces the initiation of glandular trichomes), which then allows more essential oil to be produced and stored.

Can Enzyme Concentrations in Peppermint Glandular Trichomes Be Approximated Based on Gene Expression Data?

Methods for utilizing gene expression data for modeling protein fluctuations have been developed, some of which have been applied successfully in microbial biology (for review, see Paulsson, 2005; Cinquemani et al., 2008; Ben-Tabou de-Leon and Davidson, 2009). However, data on the utility of these stochastic approaches for plant metabolism are sparse (Rios-Estepa and Lange, 2007), and we felt that it was important to find an approximation that was supported directly by experimental data. Fortunately, data on dynamic changes of gene expression and protein levels in peppermint glandular trichomes under various controlled experimental conditions were available to us. We found that there was a correlation that could be described using a logarithmic function, and the estimated changes in enzyme activities were subsequently used to approximate changes in enzyme concentrations (Supplemental Data S1). Since we did not perform any computational optimizations, the goodness of fit between simulated and experimentally determined monoterpene profiles could be used as a direct indicator of the appropriateness of our assumptions (all other known factors impacting monoterpene profiles were determined experimentally). The χ^2 statistical comparisons indicated that there was no statistically significant difference between simulated versus measured monoterpene profiles at 40 d for all experiments (Figs. 3–5), thus indicating that our modeling assumptions were valid. We were not surprised that the temporal changes of monoterpene profiles were not in full agreement with measured profiles, particularly when plants were subjected to severe stress (qualitative assessment; Figs. 3–5). Different environmental conditions and transgene insertions (and combinations thereof) will likely have as yet unknown effects on monoterpene profiles. To potentially elucidate these processes, we are planning to expand our modeling to include parameter fitting in the future, once again utilizing an iterative approach of modeling and experimental testing. Eventually, this will allow us to accurately simulate the full-time courses of all monoterpenes across multiple experimental conditions.

Assessing the Minimal Experimental Data Set for Accurate Simulations

As discussed above, we were successful in simulating monoterpene profiles under various environmental conditions and in specific transgenic lines (Figs. 3 and 4). These simulations were based on various experimental measurements and certain parameter estimations. Since we intended to utilize kinetic modeling to guide metabolic engineering efforts aimed at improving essential oil yield and composition, we evaluated to which extent experimental outcomes could be simulated based on very limited experimental data. The increased yields measured in MFS7a-GH (compared with WT-GH; 35% higher monoterpene levels) appeared to be a surprising secondary effect of transgene introgression. It was sensible to assume that MFS7a-LL plants, which were used as a test case, would have higher monoterpene levels than WT-LL, but we could not predict the magnitude of that difference, as we had no prior data on the behavior of the MFS7a line under environmental stress conditions. The measurement of essential oil yield (which turned out to be 69% higher in MFS7a-LL compared with WT-LL) was thus a requirement for accurate modeling. The differences between temporal patterns in experimentally determined and simulated profiles indicated that as yet unknown processes modulate specific enzyme activities, but it is very encouraging that the final profile at 40 d was predicted with relative accuracy (Fig. 5C).

As a test case for utilizing only previously published experimental data for simulations, we chose to investigate the transgenic line L3H20 under greenhouse conditions (L3H20-GH). The simulation (Fig. 5B, dotted line) indicated that we should observe high levels of (−)-limonene, but that was a trivial outcome (accumulation of the substrate of the enzyme whose expression is impaired in the transgenic plant). It seemed more relevant to assess how the slow increase in (−)-limonene could be explained. We thus acquired additional experimental data, in particular with regard to glandular trichome distribution. These data yielded crucial information. It was not predictable that the glandular trichome developmental program was delayed in L3H20-GH compared with WT-GH. When these experimental data were used to adjust modeling parameters, an excellent fit of experimental and simulated monoterpene profiles was observed (Fig. 5, B, broken line, and C).

Our simulations indicate that we can now account for the major factors affecting essential oil yield and composition; however, unpredictable secondary factors might affect glandular trichome initiation and development. Based on our current knowledge, it is feasible to specify a certain range defining possible outcomes of transgenic modifications. For optimizing specific traits, we would still rely on an iterative modeling approach that starts with minimal experimental data and involves the acquisition of additional data as needed. As our understanding of the regulation of essential oil biosynthesis increases, the predictive power of our models will increase as well, and less experimental data will be required for simulations. Using a descriptive approach, one attempts to fit a model to experimental data and to infer biological principles from modeling parameters. Mechanistic approaches generate models based on biological principles and then test how well these models fit experimental data sets. With our iterative approach, we are beginning to break down the line between these complementary approaches. This opens up new opportunities for guiding metabolic engineering efforts aimed at modulating monoterpenoid essential oil profiles in peppermint leaves. We are also evaluating the utility of peppermint to produce novel essential oils (in particular those accumulating highly valuable chemicals) by introducing heterologous genes from different plant species. The next generation of models will be invaluable in optimizing the performance of this "trichome factory."

MATERIALS AND METHODS

Chemicals, Plant Materials, and Growth Conditions

All chemicals were purchased from Sigma-Aldrich. Peppermint (*Mentha* × *piperita* 'Black Mitcham') plants were grown on soil (Sunshine Mix LC1; SunGro Horticulture) in a greenhouse with supplemental lighting from sodium vapor lights (850 μmol m^{-2} s^{-1} photosynthetically active radiation at plant canopy level) with a 16-h photoperiod and a temperature cycle of 27°C/21°C (day/night). Transgenic plant lines (MFS7a and L3H20) were provided by the laboratory of Dr. R. Croteau at Washington State University. The initial characterization of these transgenic lines was published previously (Mahmoud and Croteau, 2001; Mahmoud et al., 2004). Plants were watered daily with a fertilizer mix (nitrogen:phosphorus:potassium, 20:20:20 [v/v/v], plus iron chelate and micronutrients). Stress experiments were performed by (1) reducing water amounts (50% of the regular volume), (2) moving plants to a growth chamber with a 16-h photoperiod at reduced light levels (300 μmol m^{-2} s^{-1} photosynthetically active radiation at plant canopy level), and (3) combining a low-light treatment (as above) with high night temperature (30°C/30°C, day/night).

Monoterpene Analysis

Leaves were directly (without prior freezing) steam distilled and solvent extracted using 10 mL of pentane in a condenser-cooled Likens-Nickerson apparatus (Ringer et al., 2003). Monoterpenes were identified by comparison of retention times and mass spectra with those of authentic standards in gas chromatography with mass spectrometry detection. Quantification was achieved by gas chromatography with flame ionization detection based upon calibration curves with known amounts of authentic standards and normalization to the peak area of camphor as an internal standard (Ringer et al., 2003).

Glandular Trichome Distribution

The distribution of glandular trichomes on peppermint leaves was evaluated using the method described by Turner et al. (2000) with minor modifications. Briefly, leaves were cut along their blade, and each half was divided into three sampling zones (basal, middle, and apical). Both abaxial and adaxial leaf surfaces were sampled. Transmission electron microscopy grids (50 mesh, 3 mm diameter; containing 12-grid squares with an enclosed area of about 0.18 mm^2 each; Pelco International) were placed on leaf surfaces. Glandular trichome counting was performed in five grids per zone and on five different leaves. The total leaf area and the diameters of individual glandular

trichomes were calculated based on digitized images of leaves (ImageJ, an open source software developed by the National Institutes of Health) using previously described methods (Turner et al., 2000). The calculations of essential oil volume per trichome were performed as described in Supplemental Data S1.

Real-Time Quantitative PCR

Oil gland secretory cells were isolated from peppermint leaves at 15 and 30 d after leaf emergence using a previously published protocol (Lange et al., 2000). Total RNA was extracted from isolated secretory cells using the Trizol Reagent (Gibco BRL) according to the manufacturer's instructions. Total RNA (1 μg) was treated with RNase-free DNase (Fermentas Life Science), and first-strand cDNA was synthesized using reverse transcriptase (Invitrogen). RNA isolation and cDNA synthesis were carried out with three independent biological replicate samples. In a 10-μL quantitative PCR, concentrations were adjusted to 18 nM (primers), 2.5 μM [oligo(dT)s], and 0.5 mM (deoxyribonucleotide triphosphates). Reactions were performed on a 96-well optical plate at 95°C for 10 min, followed by 40 cycles of 95°C for 15 s and 60°C for 10 min (7500 Real-Time PCR system; Applied Biosystems). Fluorescence intensities of three independent measurements were normalized against the ROX reference dye. For each experimental sample, the amounts of target and endogenous control (β-actin gene; AW255057) were determined using the comparative threshold cycle (C_T) method according to the manufacturer's instructions (Applied Biosystems). The calculated average target value was subtracted from the average endogenous control value to obtain ΔC_T. First-strand cDNA obtained from RNA of wild-type secretory cells (harvested at late postsecretory stage and thus with very low expression levels of target genes) was used as the template for calibrator measurements as above. The ΔC_T of the calibrator was then subtracted from the ΔC_T of the target to obtain $-\Delta\Delta C_T$. The relative amount of target, normalized to an endogenous control and relative to the calibrator, was then calculated as relative quantitation = $2^{-\Delta\Delta C_T}$. Thus, the normalized amount of each target is expressed as a unitless number, and all quantities are expressed as an x-fold difference relative to the value obtained with the calibrator sample. Primer design for the genes of interest was performed using the Primer Express software (Applied Biosystems). The following primer pairs (obtained from Sigma-Genosys) were used (gene numbering as in Fig. 1): 1, AF019383, forward (F), 5′-AAGAAGCAGGGCTGAGTCCTAA-3′; reverse (R), 5′-TGTCCTTTCCTCCTCCAATCA-3′; 2, AF116825, F, 5′-CGGCTACCTCGACATTTTCAA-3′; R, 5′-GCGACACCGCCATTTCC-3′; 4, AF179283, F, 5′-TGTCCCACTGGTGAAGTTTACAA-3′; R, 5′-CTAGCAACACCAATGGATCAATG-3′; 6, AW255909, F, 5′-TCGACCTGTATGTTGGCA-3′; R, 5′-GATTAGGGCATCCGTAGCATTC-3′; 10, AW255536, F, 5′-CTCGCACTCAACAACTTCGTC-3′; R, 5′-CCCACGATTGTCGAAGATAGG-3′; 11, AF124817, F, 5′-CGTTCGGAGCGGGAAGA-3′; R, 5′-CAATGGAACCTCAACGTTTGC-3′; 15, EU108704, F, 5′-GCCGGAACCGATACGACTTT-3′; R, 5′-TTTTAGGGTACGCGGGTTTTT-3′; 16, AY300163, F, 5′-GGAAGATGCTTGAAGCTGTGATC-3′; R, 5′-ACTGGGAGACCATCCCACATAC-3′.

Kinetic Mathematical Modeling

Descriptions of modeling assumptions, variables, parameters, and the MATLAB source code are provided in MIRIAM-compatible format (LeNovère et al., 2005) in Supplemental Data S1. Kinetic mathematical modeling to simulate monoterpene profiles in peppermint leaves was performed according to Rios-Estepa et al. (2008), with several modifications. Briefly, we expanded the model to include the methylerythritol 4-phosphate pathway, which provides the precursors for peppermint monoterpenoid essential oil biosynthesis (Eisenreich et al., 1997). Our modified model also does not contain the factors p and q, which we had introduced to account for the fraction of PR activity affected by feedback [(+)-menthofuran] and substrate [(+)-pulegone] inhibition, respectively. Instead, a new factor, w, was introduced, which allows us to account for the very small amounts of the intermediate (+)-pulegone retained within the secretory cells (not secreted into the subcuticular oil storage cavity). We continue to utilize the factor z, which accounts for the selective retention of (+)-menthofuran in secretory cells under stress conditions. Furthermore, based on the gene expression data presented here, the enzyme concentrations used in our model were adjusted for different peppermint genotypes grown under various environmental conditions (Supplemental Data S1). A function that accounts for the developmental changes in the density of glandular trichomes was also added to the code of our model. Thus, simulations of essential oil yield and composition in individual glandular trichomes can be extrapolated to the scale of an entire leaf (Supplemental Data S1).

Supplemental Data

The following materials are available in the online version of this article.

Supplemental Data S1. Listing and description of assumptions, estimations, calculations, statistical analysis methods, and code used for mathematical modeling of peppermint essential oil profiles.

ACKNOWLEDGMENTS

We thank Dr. Rodney Croteau for permission to use transgenic lines MFS7a and L3H20, which were generated in his laboratory. We also appreciate the fact that Drs. Rodney Croteau and Edward Davis shared data prior to publication. We thank Julia Gothard-Szamosfalvi and Craig Whitney for growing plants and for assistance with operating growth chambers. We are appreciative of Dr. Glenn W. Turner's advice on experimental protocols. R.R.-E. thanks the Fulbright program and the University of Antioquia (Medellin, Colombia) for scholarships. We appreciate the feedback from two anonymous reviewers, which provided valuable advice for improving the manuscript.

Received December 15, 2009; accepted February 4, 2010; published February 10, 2010.

LITERATURE CITED

Amelunxen F (1965) Electron microscopic analysis of glandular trichomes of *Mentha piperita* L. (Translated from German.) Planta Med **13:** 457–473

Ben-Tabou de-Leon S, Davidson EH (2009) Modeling the dynamics of transcriptional gene regulatory networks for animal development. Dev Biol **325:** 317–328

Boughton AJ, Hoover K, Felton GW (2005) Methyl jasmonate application induces increased densities of glandular trichomes on tomato, *Lycopersicon esculentum*. J Chem Ecol **31:** 2211–2216

Bruggeman FJ, Westerhoff HV (2006) Approaches to biosimulation of cellular processes. J Biol Phys **32:** 273–288

Burbott AJ, Loomis WD (1967) Effects of light and temperature on the monoterpenes of peppermint. Plant Physiol **42:** 20–28

Cinquemani E, Millias-Argeitis A, Summers S, Lygeros J (2008) Stochastic dynamics of genetic networks: modeling and parameter identification. Bioinformatics **24:** 2748–2754

Clark RJ, Menary RC (1980) Environmental effects on peppermint (*Mentha piperita* L.). I. Effect of day length, photon flux density, night temperature and day temperature on the yield and composition of peppermint oil. Aust J Plant Physiol **7:** 685–692

Colson M, Pupier R, Perrin A (1993) Biomathematical analysis of the number of glandular trichomes on leaves of *Mentha* × *piperita*. (Translated from French.) Can J Bot **71:** 1202–1211

Croteau R, Davis EM, Ringer KL, Wildung MR (2005) (−)-Menthol biosynthesis and molecular genetics. Naturwissenschaften **92:** 562–577

Davis EM, Ringer KL, McConkey ME, Croteau R (2005) Monoterpene metabolism: cloning, expression, and characterization of menthone reductases from peppermint. Plant Physiol **137:** 873–881

Diemer F, Caissard JC, Moja S, Calchat JC, Jullien F (2001) Altered monoterpene composition in transgenic mint following the introduction of 4*S*-limonene synthase. Plant Physiol Biochem **39:** 603–614

Eisenreich W, Sagner S, Zenk MH, Bacher A (1997) Monoterpenoid essential oils are not of mevalonoid origin. Tetrahedron Lett **38:** 3889–3892

Eubanks LM, Poulter CD (2003) Rhodobacter capsulatus 1-deoxy-D-xylulose 5-phosphate synthase: steady-state kinetics and substrate binding. Biochemistry **42:** 1140–1149

Gershenzon J, Maffei M, Croteau R (1989) Biochemical and histochemical localization of monoterpene biosynthesis in the glandular trichomes of spearmint (*Mentha spicata*). Plant Physiol **89:** 1351–1357

Heinrich R, Rapoport TA (1974) A linear steady-state treatment of enzy-

matic chains: general properties, control and effector strength. Eur J Biochem **42:** 89–95

Hudgins JW, Christiansen E, Franceschi VR (2003) Methyl jasmonate induces changes mimicking anatomical defenses in diverse members of the Pinaceae. Tree Physiol **23:** 361–371

Hudgins JW, Christiansen E, Franceschi VR (2004) Induction of anatomically based defense responses in stems of diverse conifers by methyl jasmonate: a phylogenetic perspective. Tree Physiol **24:** 251–264

Kacser H, Burns JA (1973) The control of flux. Symp Soc Exp Biol **27:** 65–104

Krasnyansky S, May RA, Loskutov A, Ball TM, Sink KC (1999) Transformation of the limonene synthase gene into peppermint (*Mentha piperita* L.) and preliminary studies on the essential oil profiles of single transgenic plants. Theor Appl Genet **99:** 676–682

Lange BM, Wildung MR, Stauber EJ, Sanchez C, Pouchnik D, Croteau R (2000) Probing essential oil biosynthesis and secretion by functional evaluation of expressed sequence tags from mint glandular trichomes. Proc Natl Acad Sci USA **97:** 2934–2939

Le Novère N, Finney A, Hucka M, Bhalla US, Campagne F, Collado-Vides J, Crampin EJ, Halstead M, Klipp E, Mendes P, et al (2005) Minimum information requested in the annotation of biochemical models (MIRIAM). Nat Biotechnol **23:** 1509–1515

Libourel IGL, Shachar-Hill Y (2008) Metabolic flux analysis in plants: from intelligent design to rational engineering. Annu Rev Plant Biol **59:** 625–650

Llaneras F, Picó J (2008) Stoichiometric modeling of cell metabolism. J Biosci Bioeng **105:** 1–11

Mahmoud SS, Croteau R (2001) Metabolic engineering of essential oil yield and composition in mint by altering expression of deoxyxylulose phosphate reductoisomerase and menthofuran synthase. Proc Natl Acad Sci USA **98:** 8915–8920

Mahmoud SS, Williams M, Croteau R (2004) Cosuppression of limonene-3-hydroxylase in peppermint promotes accumulation of limonene in the essential oil. Phytochemistry **65:** 547–554

Martin D, Tholl D, Gershenzon J, Bohlmann J (2002) Methyl jasmonate induces traumatic resin ducts, terpenoid resin biosynthesis, and terpenoid accumulation in developing xylem of Norway spruce stems. Plant Physiol **129:** 1003–1018

McCaskill D, Gershenzon J, Croteau R (1992) Morphology and monoterpene biosynthetic capabilities of secretory cell clusters isolated from glandular trichomes of peppermint (*Mentha piperita* L.). Planta **187:** 445–454

McNeil SD, Rhodes D, Russell BL, Nuccio ML, Shachar-Hill Y, Hanson AD (2000) Metabolic modeling identifies key constraints on an engineered glycine betaine synthesis pathway in tobacco. Plant Physiol **124:** 153–162

Mendes P, Messiha H, Malys N, Hoops S (2009) Enzyme kinetics and computational modeling for systems biology. Methods Enzymol **467:** 583–599

Paulsson J (2005) Models of stochastic gene expression. Phys Life Rev **2:** 157–175

Poolman MG, Assmus HE, Fell DA (2004) Applications of metabolic modeling to plant metabolism. J Exp Bot **55:** 1177–1186

Ramos-Valdivia AC, Van der Heiden R, Verpoorte R, Camara B (1997) Purification and characterization of two isoforms of isopentenyl diphosphate isomerase from elicitor-treated *Cinchona robusta* cells. Eur J Biochem **249:** 161–170

Ringer KL, McConkey ME, Davis EM, Rushing GW, Croteau R (2003) Monoterpene double-bond reductases of the (−)-menthol biosynthetic pathway: isolation and characterization of cDNAs encoding (−)-isopiperitenone reductase and (+)-pulegone reductase of peppermint. Arch Biochem Biophys **418:** 80–92

Rios-Estepa R, Lange BM (2007) Experimental and mathematical approaches to modeling plant metabolic networks. Phytochemistry **68:** 2351–2374

Rios-Estepa R, Turner GW, Lee JM, Croteau RB, Lange BM (2008) A systems biology approach identifies the biochemical mechanisms regulating monoterpenoid essential oil composition in peppermint. Proc Natl Acad Sci USA **105:** 2818–2823

Rohdich F, Lauw S, Kaiser J, Feicht R, Kohler P, Bacher A, Eisenreich W (2006) Isoprenoid biosynthesis in plants: 2C-methyl-D-erythritol 4-phosphate synthase (IspC protein) of Arabidopsis thaliana. FEBS J **273:** 4446–4458

Rohloff J (1999) Monoterpene composition of essential oil from peppermint (*Mentha* × *piperita* L.) with regard to leaf position using solid-phase microextraction and gas chromatography/mass spectrometry analysis. J Agric Food Chem **47:** 3782–3786

Traw MB, Bergelson J (2003) Interactive effects of jasmonic acid, salicylic acid, and gibberellin on induction of trichomes in Arabidopsis. Plant Physiol **133:** 1367–1375

Turner GW, Gershenzon J, Croteau R (2000) Development of peltate glandular trichomes of peppermint (*Mentha* × *piperita* L.). Plant Physiol **124:** 655–664

van Schie CCN, Haring MA, Schuurink RC (2007) Tomato linalool synthase is induced in trichomes by jasmonic acid. Plant Mol Biol **64:** 251–263

Yoshida Y, Sano R, Wada T, Takabayashi J, Okada K (2009) Jasmonic acid control of GLABRA3 links inducible defense and trichome patterning in Arabidopsis. Development **136:** 1039–1048